

Article

Physical Properties of Polypeptide Electrospun Nanofiber Cell Culture Scaffolds on a Wettable Substrate

Donald T. Haynie ^{1,2,*}, Dhan B. Khadka ¹ and Michael C. Cross ¹

¹ Nanomedicine and Nanobiotechnology Laboratory, Department of Physics, University of South Florida, 4202 East Fowler Avenue, Tampa, FL 33620, USA;

E-Mails: dkhadka@mail.usf.edu (D.B.K.); mcross80@gmail.com (M.C.C)

² Center for Integrated Functional Materials, Department of Physics, University of South Florida, 4202 East Fowler Avenue, Tampa, FL 33620, USA

* Author to whom correspondence should be addressed; E-Mail: dhaynie@usf.edu;
Tel.: +1-813-974-7793; Fax: +1-813-974-5813.

Received: 20 April 2012; in revised form: 9 August 2012 / Accepted: 23 August 2012 /
Published: 31 August 2012

Abstract: Physical properties of poly(L-ornithine) (PLO), a polycation, poly(L-glutamic acid₄-co-L-tyrosine) (PLEY), a polyanion, and electrospun fibers made of these polymers have been determined and compared. The polymers adopted random coil-like conformations in aqueous feedstocks at neutral pH and in dehydrated cast films and fibers on glass, and the fibers comprised numerous counterions, according to spectral analysis. Adsorption of model proteins and serum proteins onto hydrated and crosslinked fibers depended on the electrical charge of the proteins and the fibers. The surface charge density of the fibers will be comparable to, but less than, the charge density on the outer leaflet of the plasma membrane of usual eukaryotic cells. The present analysis thus advances understanding of cell behavior on electrospun fiber scaffolds, a topic of considerable current interest.

Keywords: cell; electrospinning; fiber; physics; polypeptide; scaffold

1. Introduction

Electrospun fiber mats hold out promise for realizing perceived advantages of nanostructured materials in many areas, including medicine and biotechnology. Fibers can be made of biocompatible and biodegradable synthetic organic polymers. Such polymers include poly(lactide-co-glycolide) and

poly(caprolactone). Interest in electrospun materials for *in vitro* tissue culture coatings, *in vivo* medical implant device coatings and other applications is now global and likely to continue growing for the foreseeable future [1–4].

Investigators have taken a variety of approaches to increasing the desirability of electrospun materials for biomedical applications and reducing the environmental footprint of materials production [2–7]. In some cases, the polymers were polypeptides (see reference [7] for a recent review). Whether natural or biomimetic, whether pure or blended with synthetic organic polymers, these polymers can provide further advantages for compatibility, degradability, absorbability and, crucially, functionality. Most polypeptide electrospinning studies have involved purified proteins that require an organic solvent for chain entanglement [7]. Lately, interest has grown in polymer electrospinning from aqueous feedstocks [5,7,8]. Model polypeptides that have a simple amino acid sequence or composition, display little persistent structure in aqueous solution under usual conditions and therefore tend to be non-immunogenic are also receiving increasing attention (reviewed in reference [7]). Such peptides can represent different degrees of biomimicry in terms of amino acid composition and sequence and functional properties. In any case, the diameter of polypeptide fibers typically ranges from 100 nm to 2 μm , though thinner and thicker fibers are spun.

It is generally held that quantitative analysis of the physical properties of feedstock solutions, the electrospinning process and the resulting fibers will lead to advances in electrospinning technology. Deitzel *et al.* [9], Yarin *et al.* [10] and Minato *et al.* [11], for example, have studied the relationship of process variables to chain conformation and fiber spinnability, bending instability, diameter and morphology. Hohman *et al.* [12], Fridrikh *et al.* [13] and He *et al.* [14] have developed theoretical models of electrospun fibers, fiber diameter and fiber stability. The primary aim of the present study was to produce a quantitative description of physical properties of polypeptide fibers on a wettable solid support.

The synthetic model polypeptides PLO and PLEY have now been analyzed in greater depth than in our previous work [4,6]. Circular dichroism spectroscopy (CD) and Fourier transform infrared spectroscopy (FTIR) have been utilized to obtain structural information on these polymers in aqueous solution, cast films and fibers. Fiber composition has been analyzed by electron-dispersive X-ray spectroscopy (EDX). Protein adsorption has been analyzed by quantitative fluorescence microscopy. A model of key electrical properties of fibers has been described and compared to literature values for the corresponding properties of glass and cells. The surface energy of the fibers has been analyzed and compared to values for various cell culture materials. The results of this work are relevant to applications of electrospun materials in medicine and biotechnology, for example, tissue engineering scaffolds and wound healing biomaterials.

2. Experimental Section

All processes were carried out at ambient temperature and humidity unless indicated otherwise. All fiber mat properties were measured *in situ* on a glass substrate.

2.1. Polymers

PLO (153.5 kDa by viscometry and 196.8 kDa by multiple-angle laser light scattering) and PLEY (20–50 kDa by viscometry) were synthesized in solution and obtained from Sigma (USA) as lyophilized polydisperse salts. The polydispersity index, defined as the ratio of the weight-average molar mass to the number-average molar mass, or M_W/M_N , is a way of quantifying the heterogeneity of polymer length. Light scattering measures M_N ; viscometry measures the viscosity-average, M_V , not M_W . Because $M_N < M_V < M_W$, M_V/M_N can be taken as a lower bound on M_W/M_N . For PLO, $M_V/M_N \approx 1.3$ and M_V/M_N was probably less than 20% higher. For PLEY, if the number density of polymers was uniform, $M_N = 35.0$ kDa, $M_W = 37.3$ kDa, $M_V = 37.1$ kDa (for the Mark-Houwink parameter $a = 0.8$, as for semi-flexible polymers [15]) and $M_W/M_N \approx 1.1$. Typical synthetic materials have $M_W/M_N \approx 4$, a value that is often improved by size-exclusion chromatography and polymer fractionation. The polydispersity of PLO or PLY is rather unlikely to have influenced the present results. The counterions were Br^- for PLO and Na^+ for PLEY. Aqueous feedstocks for electrospinning were prepared by dissolving as-received peptide in deionized water (40% w/v or 2 mM polymer, and 50% w/v or 14 mM polymer, respectively). The feedstock solutions will therefore have consisted of three main components: water (and its ionized forms), ionized polypeptide and counterions.

2.2. Electrospinning

Fibers were prepared as described previously [4,6]. Briefly, polymer feedstock was taken up into a 1 mL syringe outfitted with a 0.5 mm blunt-end needle (Jensen Global, USA). A positive potential in the 5–20 kV range was applied to the needle with a PS/FX20P15.0-11 power supply (Glassman, USA). Fibers were collected 5–15 cm from the spinneret on a glass plate on top of a grounded sheet of metal or on a sheet of 60 Ω/in^2 indium tin oxide-coated poly(ethyleneterephthalate) (ITO-PET; Sigma-Aldrich). The feedstock flow rate was not regulated.

2.3. Crosslinking

Two methods were utilized for *in situ* polymer crosslinking at ambient temperature: Exposure to glutaraldehyde vapor (25% w/v in water; Sigma) for PLO [4], and immersion in 50 mM 1-ethyl-3-(3-dimethylaminopropyl) carbodiimide (EDC; Thermo Scientific, USA) in 90% ethanol/10% water for PLEY [6]. Relevant details of the chemistry now follow. The symmetrical glutaraldehyde molecule will have reacted with amino groups in two ornithine side chains or, with much lower probability, *N*-termini, yielding no change in the number of amide groups present. As to EDC, a symmetrical diimide, the most likely reaction in this study will have involved the carboxylate moieties of two glutamic acid side chains. The resulting acid anhydrides, however, will have been unstable in aqueous solution. Formation of a stable crosslink, a peptide bond, will have required an EDC molecule to react with a glutamate side chain and the resulting *O*-acylisourea intermediate with an amino terminus; *N*-termini are the only amino groups in PLEY. The byproduct of this reaction will have been a soluble urea derivative. Additional stable crosslinks may have formed between the phenolic oxygen atoms of tyrosinate residues and *N*-termini, albeit with lower probability. Following crosslinking, PLO and PLEY fiber mesh samples were rinsed extensively with aqueous solution at neutral pH. Residual

O-acylisourea intermediates, whether formed with glutamic acid or tyrosine, will have been unstable in aqueous solution; *N*-hydroxysulfosuccinimide (sulfo-NHS) was not utilized for intermediate stabilization; failure to react with an amine will have resulted in hydrolysis, regenerating glutamate or tyrosinate and releasing an *N*-unsubstituted urea molecule to solution.

2.4. Dye Labeling and Protein Adsorption

Model proteins were assayed for adsorption onto fibers versus glass. Visualization of adsorbed material was enabled by labeling with fluorescein isothiocyanate (FITC), which is selective for free amino groups; no sulfhydryl groups were present. The test species were serum proteins, FITC-labeled hen egg white lysozyme (FITC-HEWL; Sigma) in phosphate-buffered saline (PBS) and FITC-labeled bovine serum albumin (FITC-BSA; Sigma) in PBS. For PLEY, fibers and serum proteins were labeled *in situ*; HEWL and BSA, *ex situ*. For PLO, serum proteins, HEWL and BSA were labeled *ex situ*.

All labeling reactions were carried out overnight at 4 °C, the dye concentration was 1 mg/mL in dimethylsulfoxide, and the buffer was 20 mM sodium carbonate, pH 9. For HEWL and BSA labeling, the protein concentration was 2 mg/mL. Carbonate buffer was diluted 1:100 in PBS after labeling, and the final protein concentration was adjusted to 2 mg/mL, the approximate concentration of BSA in cell culture medium; 10% fetal bovine serum (FBS) has a protein concentration of 3–4.5 mg/mL, and the concentration of BSA is 0.69–1.52 mg/mL [16]. For direct labeling of PLEY fibers, FITC will have reacted with free amino termini. Non-specific adsorption of FITC onto fibers or glass may also have been strong enough to remain bound after rinsing. For PLO fibers, too many free amino groups were present in side chains for direct labeling. Some PLEY fiber samples were incubated overnight with fibroblast culture medium (Lonza, USA) supplemented with 10% FBS. These samples were then rinsed with PBS and labeled with FITC as described above. FITC will have reacted with free amino groups on bound serum proteins and amino termini in fibers. All fiber samples were rinsed with deionized water for visualization and image capture by fluorescence microscopy.

2.5. Spectroscopy and Microscopy

2.5.1. CD

Far-UV spectra of PLO and PLEY were collected with an Aviv Biomedical 215 instrument (USA). 5 scans were averaged for measurement over a range of 190–270 nm at a rate of 1 nm/s, a step size of 1 nm and a bandwidth of 1 nm. The peptide concentration was 1.3 μM for PLO and 5.7 μM for PLEY. The path length was 1.0 cm. The temperature was 25 °C.

2.5.2. FTIR

A Jasco 4100 instrument (Japan) was utilized to obtain FTIR spectra of cast films, fibers and crosslinked fibers of PLO and PLEY on ITO-PET over the 1000 to 4000 cm⁻¹ range in attenuated total reflectance mode. The ATR accessory (Harrick Scientific, USA) was equipped with a ZnSe crystal. The bandwidth was 4 cm⁻¹; 256 spectra were averaged in each case.

2.5.3. EDX

Spectra of glass, PLO fibers on glass and PLEY fibers glass were collected with an INCA X-sight 7582M energy-dispersive spectrometer (Oxford Instruments, UK) mounted on a JSM-6390LV scanning electron microscope (SEM; JEOL, Japan). The fiber samples were not crosslinked. The working distance was 10 mm, and the accelerating voltage was 15 kV. Copper tape was utilized as a calibration standard without changing focus, spot size or accelerating voltage.

2.5.4. Microscopy

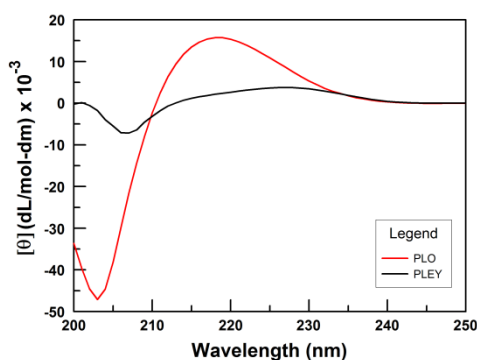
Bright-field and fluorescence micrographs of fibers after protein adsorption were obtained with a Zeiss Axiovert 200 M inverted microscope (Germany) equipped with an incandescent source, a mercury vapor source, a filter set, a 10× objective lens and a Roper Scientific MicroMAX System CCD camera (USA). The excitation wavelength was 488 nm. A JEOL JSM-6390LV scanning electron microscope (Japan) was utilized for fiber morphometry after metalizing samples with 10 nm of gold. The accelerating potential was 30 kV.

3. Results

3.1. Polymer Conformation

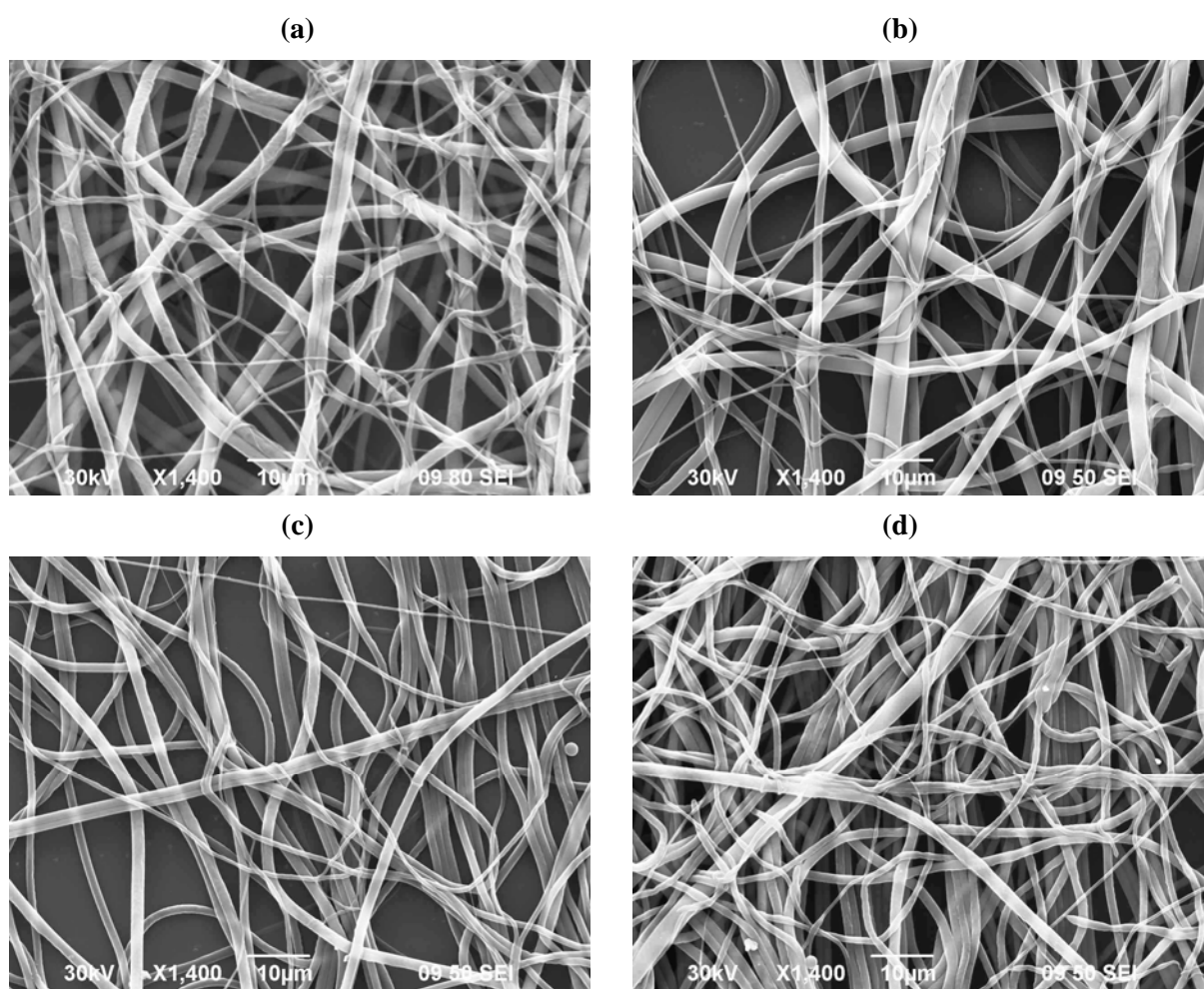
PLO and PLEY chains will have been extensively ionized in water at 25 °C and neutral pH [17,18]. Both polymers adopted a mostly random coil conformation under these conditions, according to analysis by CD (Figure 1). Evidence is provided by the large narrow absorption band near 205 nm, which is a general indicator of a disordered polypeptide backbone, and by the absence of a negative band in the 210–220 nm range, which would be expected for α helix or β sheet [19]. The main difference between the PLO and PLEY spectra is the contribution of the tyrosine rings in PLEY. The molar absorptivity of the tyrosine side chain is *ca.* 8000 M⁻¹ cm⁻¹ at 225 nm [20], and this can influence the CD signal to within about 25 nm of the center of the band [21]. What is important here is that both polymers were mostly unstructured in the aqueous feedstock.

Figure 1. Far-UV dichroic spectra of polymers in water. Poly(ornithine) (red), poly(glutamic acid, tyrosine) (black). The polymer concentration, 0.02 mg/mL in each case, was *ca.* 2000× lower than for electrospinning.



Electrospinning the polymer solutions represented by Figure 1 produced fibers represented by the scanning electron micrographs shown in Figure 2. Panels a and b show PLEY fibers before and after crosslinking; panels c and d, PLO fibers. Fiber diameter ranged from ~ 0.1 to several microns, based on analysis of digital micrographs. Mat thickness, a function of the fiber production rate and time, was always under $50\ \mu\text{m}$ here. There was no obvious change in fiber morphology on crosslinking.

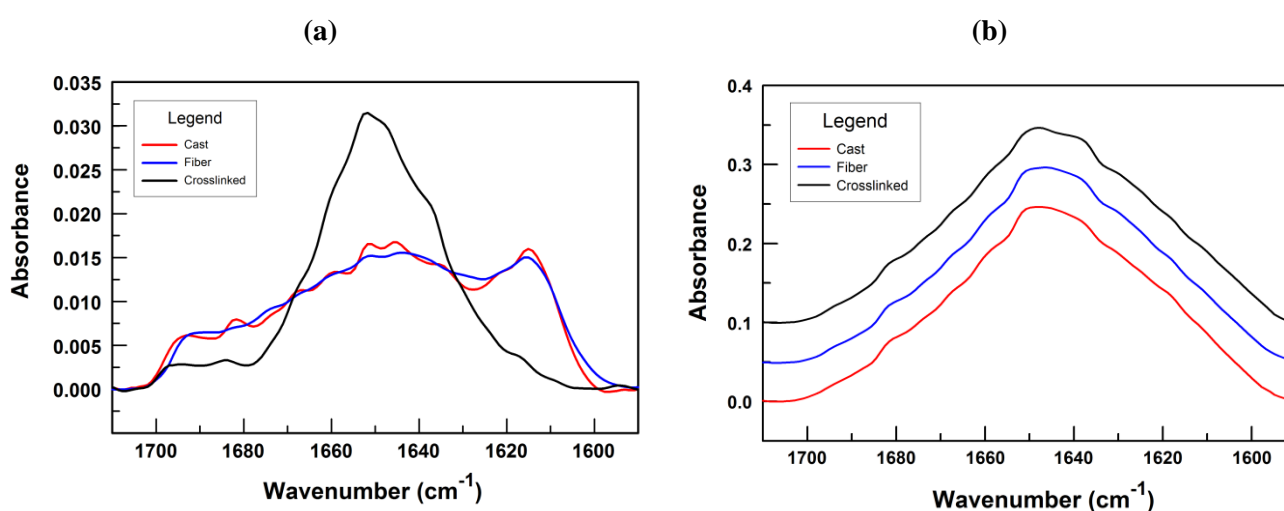
Figure 2. Fiber mat morphology. PLEY: (a) Non-crosslinked; (b) Crosslinked. PLO: (c) Non-crosslinked; (d) Crosslinked. All micrographs were obtained at $1400\times$ magnification and 30 kV accelerating potential.



Analysis of the amide I region of the IR spectra of fibers prepared as in Figure 2 showed that most polymers were in a random coil conformation prior to crosslinking, in PLO and in PLEY. Key differences were evident, however, on closer comparison. Resonances in the amide I region are primarily due to stretching vibrations of main-chain carbonyl groups. For PLEY, the close similarity of the fiber spectrum to the cast film spectrum suggests that molecules lacked a preferred orientation in fibers and, therefore, that polymer chains in the fiber interior had little regular structure (Figure 3a). Some residues evidently adopted a β sheet conformation prior to crosslinking, however, based on the amplitude, resolvability and width of absorbance bands in the amide I region, especially near $1651\ \text{cm}^{-1}$ (coil), $1617\ \text{cm}^{-1}$ (β sheet) and $1681\ \text{cm}^{-1}$ (turn) [22,23]. β sheets are characterized by

hydrogen bonds formed between polymer backbone amide groups and carbonyl groups. Here, β sheet formation will presumably have made a favorable contribution to the enthalpy of the polymer system during solvent evaporation; it may also have influenced the entropy by releasing to bulk solution and then to the vapor phase water molecules initially hydrogen bonded to donors and acceptors in the polymer backbone.

Figure 3. Infrared analysis of cast films and fibers. Cast film (red), fibers (blue) and crosslinked fibers (black). All but the amide I envelope was subtracted from the spectra during baseline treatment. (a) PLEY; (b) PLO. There is a vertical offset of 0.05 between the spectra in this panel.



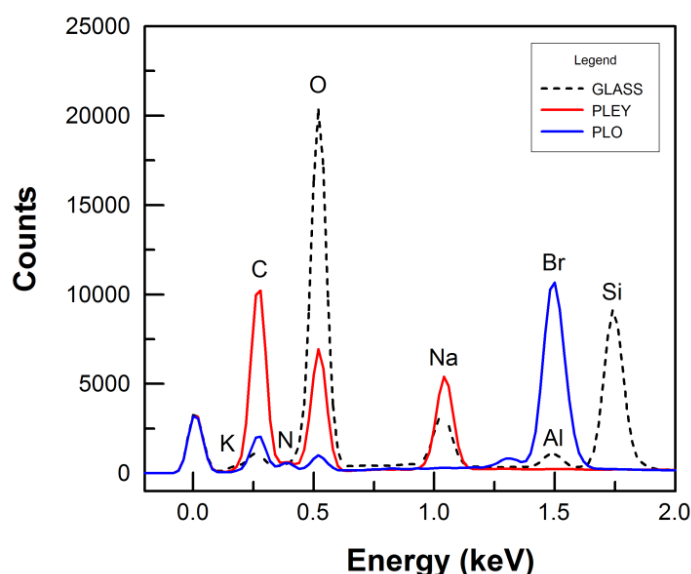
Crosslinking is necessary to make PLEY fibers and PLO fibers water-insoluble [4,6]. For PLEY, the EDC crosslinker will have reacted with the carboxylate group in a glutamate side chain and an *N*-terminal amino group. This will have increased the number of peptide bonds present, but only by a maximum of 1 per polymer chain; a mere 0.5% rise in the number of carbonyl groups contributing to the amide I spectrum for the PLEY molecules of this study. The β -sheet bands around 1617 cm^{-1} and 1682 cm^{-1} decreased and the random-coil band around 1651 cm^{-1} increased on crosslinking. The large change in shape of the amide I envelope (Figure 3a) must therefore be due to a large change in the average conformation of polymers in the fibers—despite a lack of change in fiber morphology (Figure 2a,b). The crosslinking reaction evidently decreased the ability of PLEY molecules to form β sheets in fibers. Rinsing crosslinked fibers in aqueous solution will presumably have reversed any changes in the average backbone conformation of PLEY due to ethanol, the solvent for EDC. The spectral changes on crosslinking were *internal* to the fibers.

As to PLO, crosslinking depended on the reactivity of side chains, just as for PLEY. Each end of a glutaraldehyde molecule will have reacted with a side-chain amino group, forming an imine. Unlike PLEY, PLO showed almost no difference between the cast film, fiber and crosslinked fiber spectra (Figure 3b). The largest peak in the spectra, at 1651 cm^{-1} , can be assigned to random coil. A second large peak, at *ca.* 1640 cm^{-1} , may be due to α helix. Both peaks are very broad, consistent with both a broad range of dihedral angles in any secondary structure present and limited thermostability [22]. In any case, most residues had random backbone dihedral angles in PLO fibers and in PLEY fibers after crosslinking.

3.2. Fiber Stability and Composition

Both PLO and PLEY fibers display considerable post-spinning stability in dry air in the absence of crosslinking [4,6]. This alone implies that counterions will be present inside the fibers, which would otherwise be very unstable due to charge repulsion. EDX analysis has confirmed this view (Figure 4). For PLEY, the relative abundance of carbon, oxygen and sodium atoms was respectively 62.3%, 56.7% and 15.4% for the fiber sample on glass and 6.4%, 44.4% and 3.9% for the glass control.

Figure 4. Energy-dispersive X-ray spectroscopic analysis of fibers. Spectra of glass, PLEY fibers on glass and PLO fibers on glass. Note the relative sizes of the oxygen, sodium and silicon peaks. The silicon peak occurs at *ca.* 1.8 keV. In the fibers samples, the silicon peak is lost in the noise; bare glass contributes relatively little to the measured values; the most prominent peaks are for carbon and oxygen (PLEY and PLO), sodium (PLEY) and bromide (PLO).



The abundance of silicon was 9.1% and <1%, respectively. These measurements translate into atomic ratios of 16.3 for C:N, 1.1 for C:O and 4.1 for O:Na for PLEY fibers on glass. The corresponding data for PLO are shown in spectral form in Figure 4.

The EDX results can be compared with predictions based on polymer structure. For PLEY, for instance, there were 30 C atoms for every 5 of N, 14 of O and 4 of Na, assuming complete ionization of glutamic acid side chains, no ionization of tyrosine side chains and complete charge compensation by counterions. The corresponding ratios are 6 for C:N, 2.1 for C:O and 7.5 for C:Na. The difference from the corresponding measured value may be attributed to a deviation of Glu:Tyr from 4.0:1.0, incomplete side chain ionization, incomplete removal of excess Na^+ from PLEY prior to lyophilization or substitution of H_3O^+ for Na^+ in PLEY fibers. PLO could not be analyzed in this way because the extent of crosslinking was not determined. The main point here is that Na^+ was abundant in PLEY fibers and Br^- was in PLO fibers.

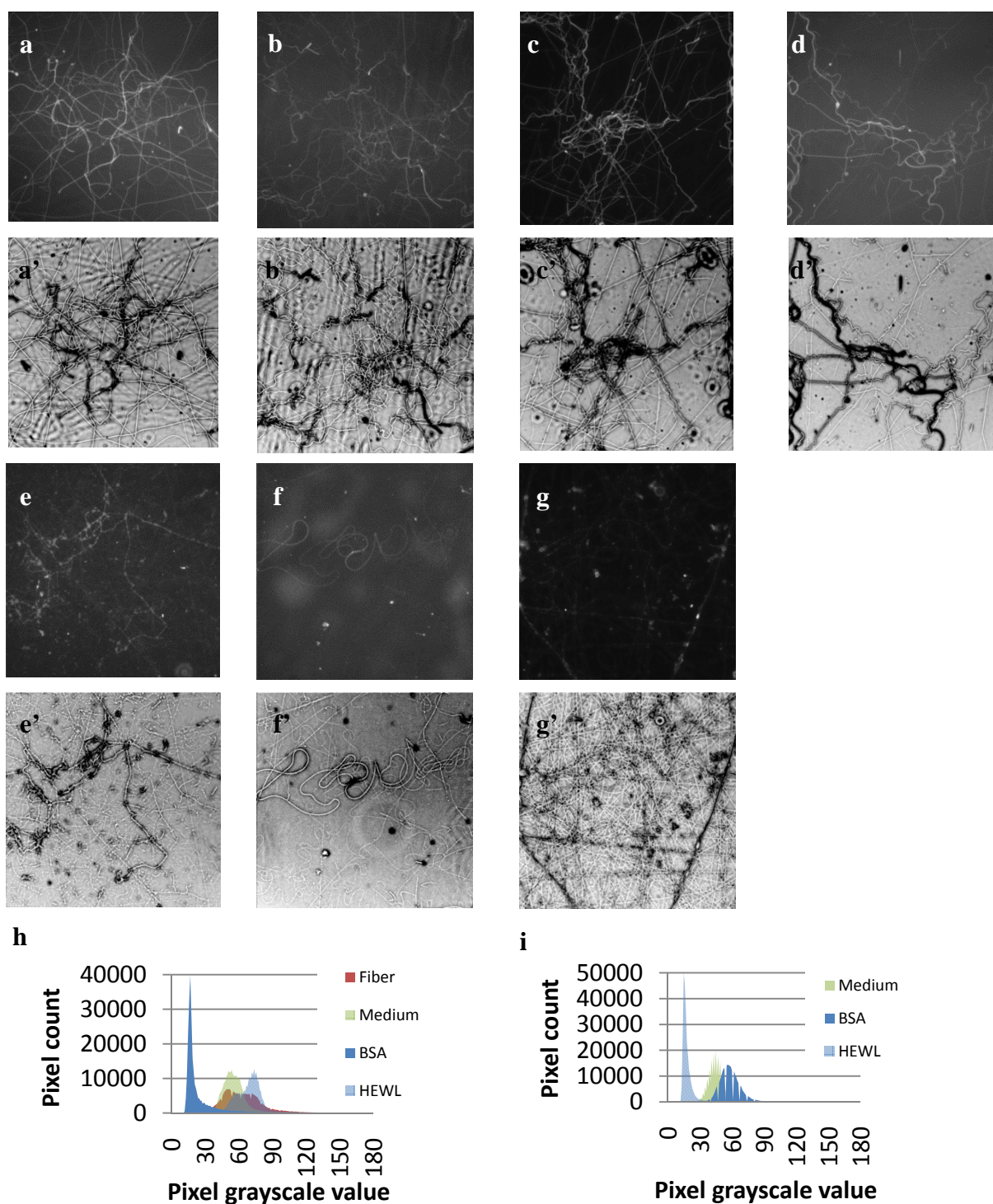
3.3. Protein Adsorption

Serum protein adsorption onto the surface of a biomaterial influences the foreign body response and therefore clinical complications arising from implantation. Protein binding affinity to a material is determined by Coulomb forces and van der Waals interactions. Adsorption of the model proteins HEWL and BSA and serum proteins onto PLEY fibers and PLO fibers has been studied here. Unmodified HEWL has an isoelectric point of 11.5 and therefore a positive net charge at neutral pH [24]; BSA has an isoelectric point of 4.7 and therefore a negative net charge at neutral pH [25]. Limited FITC labeling will not have altered either isoelectric point by a significant margin.

Figure 5a shows PLEY fibers after direct labeling with FITC. Dye molecules will have become conjugated to *N*-termini still available after EDC crosslinking or bound non-specifically to fibers or glass. PLEY fibers were scarcely more densely coated with FITC-labeled serum proteins than was the glass substrate, according to Figure 5b. Many of the proteins adsorbed onto fibers will have been positively charged by virtue of ionized lysine residues. This amino acid, which has a primary amino group in the side chain, is labeled by FITC. The high background staining evident in panels a and b can be attributed to *in situ* labeling and non-specific FITC adsorption. Contrast in the FITC-BSA micrograph (Figure 5c) is comparatively high, and the overall signal intensity is low. This suggests that BSA had greater affinity for fibers than glass, despite the negative charge on PLEY. BSA is well-known to be “sticky”, to bind non-specifically to many materials; the hydrophobic component of binding may have been greater for fibers than glass. Panel d shows the result of incubating FITC-HEWL with PLEY fibers. This cationic protein was expected to bind both PLEY fibers and glass. The contrast between fibers and glass was correspondingly low. A hydrophobic contribution to HEWL binding cannot be excluded. Similar results were obtained for PLO binding to fibers.

Figure 5h,i summarizes the fluorescence data for PLEY fibers (panels a–d) and PLO fibers (panels e–g) and quantify fluorescence as distributions of pixel intensities. BSA binding to PLEY fibers resulted in a high frequency of low grayscale values (light intensities). This makes sense because both BSA and PLEY were anionic in the experiments. The maximum in the BSA distribution was at a much higher grayscale value for PLO fibers. Just the opposite was found for HEWL, which was cationic in the experiments. The inward spikes in the BSA profile in Figure 5i are image processing artifacts that arose from increasing the contrast between the fiber signal and the glass signal; the shape of the envelope was not altered. The protein adsorption data are substantially explained by the sign of charge of the glass, the sign of charge and relative charge density of the fibers and the sign of charge of the model proteins. Evidently, serum contains proteins that will bind to either positive fibers or negative fibers having the surface density of charge of the fibers studied here.

Figure 5. Protein adsorption onto fibers or glass. Proteins became deposited during overnight incubation at 37 °C. Bright-field images have been inverted and equalized to increase contrast; there was no processing of the fluorescence micrographs. **(a, a')** Fluorescein (FITC)-labeled PLEY fibers. FITC-labeled proteins on **(b, b')** PLEY fibers or **(e, e')** PLO fibers after deposition from culture medium. FITC-bovine serum albumin on **(c, c')** PLEY fibers or **(f, f')** PLO fibers. FITC-hen egg white lysozyme on **(d, d')** PLEY fibers or **(g, g')** PLO fibers; **(h)** Grayscale histogram of pixel intensities for fluorescence micrographs in **(a–d)**; **(i)** Grayscale histogram of pixel intensities for fluorescence micrographs in **(e–g)**.



4. Discussion

4.1. Fiber Formation, Composition and Structure

Chain entanglement is a major requirement for fiber spinning from a polymer feedstock [26]. Here, the feedstock concentration was ~40% (w/v) for PLO and ~50% for PLEY. The corresponding concentration of small counterions was ~1 M in each case, assuming the charge per residue at neutral pH was *ca.* +0.8 for PLO and *ca.* -0.8 for PLEY [27]. Charge repulsion between polymer molecules will have been significant, though at close range only. Such considerations suggest that PLO chains and PLEY chains will behave as statistical coils in aqueous solution at neutral pH below the solubility limit. The spectral data in Figure 1 show that PLO formed little helical structure in water at neutral pH. Even at strongly basic pH, PLO will adopt only a modest amount of helical structure, even though poly(lysine), which differs from PLO by just one extra methylene group in the side chain, converts to helix when the side-chain amino groups are deionized [17]. Poly(glutamic acid) forms α -helical structure at acidic pH, where the side-chain carboxyl groups are deionized, but the polymer is mostly unstructured at neutral pH, where the side chains are protonated [18]. PLEY, like poly(glutamic acid), displayed a random coil-like conformation in water at neutral pH (Figure 1).

Polymer conformation in solution may be compared with conformation in a cast film or in fibers. The IR data in Figure 3 indicate that a large proportion of residues in PLEY molecules participated in β -sheet structure in the cast film and in fibers prior to crosslinking. Bands at 1617 cm^{-1} and 1681 cm^{-1} support the claim. Similarities and differences with respect to globular proteins and amyloid fibrils are worth mentioning here for the sake of interpreting the IR data. In a recent study by Zandomeneghi *et al.*, for example, amide I' data were reported for transthyretin, a β -sheet protein [28]. (The measurements were made in D₂O rather than water; the change in isotope will have had little effect on the shape of the distribution of stretching vibrations of main-chain carbonyl groups.) The native protein in solution displayed a broad amide I' envelope with a maximum at 1630 cm^{-1} . Fibrils of this protein, by contrast, showed a large and narrow band at 1615 cm^{-1} and a corresponding peak of lower intensity at 1684 cm^{-1} , similar to amyloid fibrils. A close resemblance of the transthyretin fibril and amyloid fibril IR bands to the PLEY data in Figure 3 is evident. Zandomeneghi *et al.* further interpreted their results as follows. β -sheet residues will have greater structural homogeneity in the core of amyloid fibrils than in native proteins. Amyloid fibrils correspond to very low free energy states, much deeper than the potential wells of native proteins, even if the polymers are kinetically trapped in amyloid material. A large right-handed β -sheet twist angle correlated with a high wavenumber maximum for the amide I' band, and the amide I' band wavenumber maximum correlated with the average number of strands per β sheet in transthyretin. Protein structure analysis by Richardson concluded that β sheets with fewer strands tend to have larger average twist angles [29]. No significant shift in the amide I band of the β -sheet protein lithostathine occurred on oligomerization into non-amyloid fibrils [30]. Zandomeneghi *et al.* proposed on these grounds that IR analysis, and more specifically a shift of the amide I band from about 1630 cm^{-1} to about 1615 cm^{-1} and the simultaneous appearance of a band at about 1684 cm^{-1} , could be a diagnostic for amyloid fibril formation [28]. The data in Figure 3 show that bands at 1615 cm^{-1} and 1684 cm^{-1} are not unambiguous indicators of amyloid fibril formation.

The band shift from about 1630 cm^{-1} to about 1615 cm^{-1} merits further attention for reasons that will become evident presently. Dimerization of a carboxylic acid, for example, propanoic acid in CCl_4 , can decrease the vibrational frequency of the carbonyl oxygen by as much as 45 cm^{-1} [31]. A low wavenumber maximum for a β sheet, as in transthyretin fibrils and PLEY cast films or fibers, may therefore represent an average structure in which backbone hydrogen bonds deepen the free energy well more than in native proteins. The energetic unfavorability of an increased average twist angle in a β strand in a native protein can apparently be more than offset by other kinds of interaction, for example, hydrophobic contacts between side chains. Such interactions are less probable in a cast film or electrospun fiber of PLO or PLEY, because the amino acid sequence diversity of these molecules is vastly lower than in a protein-encoding polypeptide and there are therefore vastly fewer distinguishable ways in which side chains can pack together, especially under the constraint of forming a large number of energetically significant interactions with counterions, as in the present study (Figure 4). PLEY chain oligomerization was presumably uncoordinated and in any case rapid during the dehydration of polymer jets or cast films. Both processes were nevertheless sufficient to give rise to resonances near 1615 cm^{-1} and 1680 cm^{-1} (Figure 3). Therefore, these bands cannot be considered unambiguous markers of amyloid fibrils. Further, PLEY residues in a β sheet conformation are likely to have but modest average right-handed twist angles. It is less clear whether the available fiber data also provide evidence for a relatively large average number of strands per β sheet.

4.2. Crosslinking

The data in Figure 3 also show that the EDC crosslinking reaction disrupted the β sheets formed between PLEY molecules during fiber production or further dehydration on the collector. The enthalpy of hydrogen bond formation will be relatively small, $\sim 4\text{ kJ/mol}$ [32], close to thermal energy at $25\text{ }^\circ\text{C}$. In PLEY fibers, perhaps 1 in 4 of all residues was in a β sheet conformation prior to crosslinking, judging by the area of the resonance at 1617 cm^{-1} *vis-à-vis* the total area of the amide I envelope. The distribution of β -strand lengths was probably broad, some chains of ideal backbone geometry will not have formed a β sheet, some β sheets will have comprised non-ideal backbone angles, and the composition of individual β sheets will probably have fluctuated more rapidly than in amyloid fibrils. It is probable that the mean number of consecutive residues in a β strand was modest for the same reason that many relatively small α helices are more probable than one long helix in a long chain of poly(lysine) or poly(glutamic acid): Entropy maximization [33]. It is likely, therefore, that little energy was required to disrupt most β sheets in PLEY fibers during EDC crosslinking. This energy will have been provided by thermal fluctuations and, possibly, the interaction of ethanol with the fibers. It was not determined whether crosslinking involved polymers throughout the fiber or only on the fiber surface.

4.3. Electrical Properties

Elementary electrical properties of PLO and PLEY fibers are usefully discussed here for the sake of interpreting the data in Figure 5. Such properties are of interest not only for their own sake but also for a variety of potential applications of electrospun materials. The surface charge density and the sign of the net charge of a fiber mat could determine its utility, for instance, for ion exchange in a filter application or for protein adsorption in a tissue culture scaffold application or an implantable

biomaterial application. Cell-substrate interactions in serum-supplemented tissue culture *in vitro* are relevant to cell adhesion, proliferation, morphology, activation, differentiation and senescence [34]. *In vivo*, serum protein adsorption onto a biomaterial plays a crucial role in the foreign body response, leading in turn to the broad range of clinical complications associated with device implantation [35].

The surface charge density for glass and for fibers can be compared as follows. The properties of glass are relevant here because it was the material on which fibers were collected in the present study. For glass in contact with deionized water, the effective charge density is $\sim 2 \times 10^3$ electronic charges μm^{-2} [36,37]. This value will be lower in a physiological buffer, for example cell culture medium, which has a high ionic strength. As to fibers, assuming a density matching that of small globular proteins ($\sim 1.45 \text{ g/cm}^3$; reference [38]), the outermost 5 Å of a 1 μm radius fiber (confer Figure 2) with a length of 1 μm will have a mass of $\sim 4.4 \text{ fg}$. (The thickness of the fiber surface in which side chains will contribute to the net charge of the fiber must be estimated in the absence of additional data.) The mass fraction of Glu in PLEY is 0.79 (assuming complete charge compensation with Na^+), giving $\sim 14 \times 10^6$ Glu side chains on the surface per 1 μm of fiber. The surface density of charge will then be $\sim 2.2 \times 10^6$ electronic charges μm^{-2} . This value should probably be taken as an upper bound, as the fibers are not likely to be as dense as small globular proteins, even after crosslinking, a small proportion of glutamic acid side chains will be lost on EDC crosslinking, and some unreacted glutamate side chains may be protonated, even at pH 7.4. The surface charge density will be of similar magnitude for PLO, but of course the sign of charge must be just the opposite. The point here is that the surface charge density on a PLO fiber or a PLEY fiber will be greater than the surface charge density on glass.

Now, $\sigma_G \approx \sigma_F/1100$, where the subscripts signify glass and fiber. Taking the nominal diameter of a well-spread adhesive cell to be 50 μm , the charge on the corresponding surface area of glass will be $Q_G \approx (2 \times 10^3 \text{ electronic charges}/\mu\text{m}^2)/[\pi (25 \mu\text{m})^2] \approx 1$ electronic charge. $Q_F \approx 1100$ electronic charges for the same surface area. The field strength in air due to glass will be $E_G = \sigma/\epsilon \approx 3.6 \times 10^{-5} \text{ N/C}$ at any distance from the surface (the field lines will be perpendicular to the surface and parallel to each other to the extent that glass is planar) and the field strength due to a fiber with a radius of 1 μm will be $E_F \approx 4000 \times 10^{-5} \text{ N/C}$ at the fiber surface. The fields will be about 80-fold smaller due to water, which has a high relative permittivity, and smaller still and strongly distance-dependent with salt present, as in cell culture medium, due to Debye-Hückel screening; the Debye length, the distance over which the electrical potential falls by a factor of $1/e$, is $\sim 1 \text{ nm}$ for a 1:1 electrolyte solution at 100 mM. In summary, thicker fibers will influence the local electric field more than thinner fibers, but only close to the fiber surface; charge screening will ensure that the field is negligible farther away.

Five points of contact between the foregoing electrostatic calculations, the experimental results of this work and cell culture applications of electrospun fibers will now be discussed in turn. One, the calculated upper bound on the surface charge density of PLEY or PLO fibers was $\sim 2.2 \times 10^6$ electronic charges μm^{-2} ($\sim 3.5 \times 10^{-13} \text{ C}/\mu\text{m}^2$). Surface charge is known to influence different aspects of adhesive cell behavior. The molecular composition of the membrane (sialic acid is a major contributor) and the pH and composition of the surrounding medium together give cells a negative surface charge. Curtis *et al.* [39] have observed that, whereas surfaces bearing cations are very adhesive for cells [40], adhesion of red blood cells on anionic surfaces decreases as charge density decreases [41]. This suggests that nucleated cell adhesion could be greater on fibers than glass after topographical

differences were accounted for. Separate work has found that fibronectin, a prominent component of the extracellular matrix and serum, undergoes a transition from monolayer to multilayer adsorption on sulfonated poly(styrene) at a surface charge density above $3 \times 10^{10} \text{ C}/\mu\text{m}^2$ and forms fibrillar networks beyond $8 \times 10^{10} \text{ C}/\mu\text{m}^2$ [42]. These charge density values are many orders of magnitude greater than the calculated charge density of PLEY fibers or PLO fibers, so monolayer adsorption of fibronectin and other serum proteins is probable.

Two, if a cell can sense the electric field of glass, the cell may also be able to distinguish between PLEY or PLO fibers of different diameter. Surface charge density will be largely independent of fiber diameter, because the typical fiber radius is much greater than the length scale of an amino acid side chain. The net surface charge on a given length of fiber will therefore be higher for a thick fiber than a thin one, and the electric field will be higher for the thick fiber at the same perpendicular distance from the fiber axis. The mechanisms whereby a cell might detect differences in surface charge density are not well understood (see below).

Three, anionic fibers will attract not only Na^+ and other small counterions but also cationic serum proteins (Figure 5). The serum proteins that became bound to fibers or glass during overnight incubation with culture medium therefore depended on the composition of serum. The binding affinity and therefore the equilibrium ratio of bound versus free proteins will have varied with the net charge on the proteins at neutral pH. A cluster of acidic or basic residues on a protein may also have influenced binding, enabling an anionic protein, say, to bind an anionic fiber. Many adhesive cells, including fibroblasts, attach more readily to poly(lysine)-coated glass than glass, and PLO fibers will presumably attract anionic serum proteins as readily as PLEY fibers bind cationic serum proteins. The data in Figure 5 are consistent with this view.

Four, application of a static external electric field to fibroblasts in aqueous cell culture medium reportedly makes them elongate, orienting their bodies, actin stress fibers and microtubules perpendicular to the direction of the field [43]. Within the aqueous medium, the field will be small, owing to the polarizability of water, and there will be a current of mobile ions. The presumed cellular mechanisms involved in responding to the applied field are varied and complex: Interactions with sensors located at the cell membrane, the iontophoresis of receptors, channels and other molecules, and the separation of charged membrane components are possible explanations [44]. Cell reorientation on application of an external field of 5 V/cm is essentially complete after 3 h. This field, it should be noted, is ~ 3 orders of magnitude larger than that calculated for PLEY fibers or PLO fibers in air.

Five, many cells, including fibroblasts, display net migration toward the cathode, the negative pole of an applied external field. Directed fibroblast migration occurs at applied fields as low as 0.1 V/cm in three-dimensional collagen gels but not conventional two-dimensional culture [45]. This field magnitude is thought to be relevant to embryonic development [46], healthy epithelial tissue function and wound healing in response to epithelial cell disruption [47]. For comparison, cell electroporation for drug delivery is achieved with external fields $\sim 10^5$ larger [48], and the electric field on the surface of a PLEY or PLO fiber in air is $\sim 10^3$ smaller. PLEY is negatively charged.

4.4. Maximum Charge Density on an Unmodified Protein Fiber

The surface charge density calculation for PLEY or PLO fibers may be utilized to estimate the maximum surface charge density on a protein or peptide fiber in the absence of post-translational modification. The qualification is needed because phosphorylation of side chains can significantly change the net charge on a protein. The mass fraction of glutamic acid in a PLEY fiber is ~ 0.8 . What if fibers were made of polypeptides that were completely ionized? Taking 5 Å within the fiber surface as the limit for uncompensated side chain ionization, the maximum charge density would be $\sim 3 \times 10^6$ electronic charges μm^{-2} for a mass density like that of a small globular protein. Essentially the same value is obtained by different reasoning. Let all polymer molecules on a polypeptide fiber surface have anti-parallel β -sheet geometry, neglect backbone twist, and let the surface formed by the β sheet coincide with the surface of the fiber. Successive side chains will point above and below the fiber surface. There will be ~ 1 electronic charge for every 30 Å of surface, or 3.3×10^6 electronic charges μm^{-2} . The value found above for the surface charge density of PLEY or PLO fibers, $\sim 2.2 \times 10^6$ electronic charges μm^{-2} , is therefore of the same order of magnitude as the theoretical maximum on a protein- or peptide-based material. These values may be compared with experimental data for cells. The surface charge density on red blood cells is $\sim 2.8 \times 10^5$ electronic charges μm^{-2} [49], and for other eukaryotic cells it is as high as $\sim 1.3 \times 10^8$ electronic charges μm^{-2} [50]. The maximum protein fiber surface charge density approaches but probably does not exceed the charge density of a membrane in a living cell. The maximum value is unlikely to be realized in a living organism. For a strongly anionic polypeptide could compete with DNA for DNA-binding proteins and thus interfere with regulation of gene expression; and a strongly cationic polypeptide could form an interpolyelectrolyte complex with DNA and thus interfere with gene expression and possibly DNA replication, and it could disrupt membrane structure.

Finally, if the surface charge density of a PLEY or a PLO fiber does depend on fiber radius, there are only two possibilities. A lower charge density for a thick fiber would imply greater charge repulsion on a thin fiber closer to the structure-imposed limit of surface charge density. This must be considered implausible. If the surface density of ionizable groups is essentially independent of fiber radius, there will be a larger driving force for side chain neutralization on a thin fiber, lowering the effective surface density of charge. Therefore, the surface charge density can only be higher on a thick fiber. The field of a thick fiber will in any case exceed that of a thin fiber at a given distance from the fiber axis.

5. Conclusions

Key physical properties of polypeptides in solution and peptide-based electrospun fibers on glass have been analyzed. PLEY and PLO were random coil-like in aqueous solution, whereas in fibers and cast films, a large fraction of residues in PLEY but not PLO adopted a β -sheet conformation prior to crosslinking. Significant IR absorption bands near 1615 cm^{-1} and 1680 cm^{-1} were displayed by cast films of PLEY, so the bands cannot be taken as unambiguous indicators of amyloid fibril formation. Crosslinking PLEY fibers with a diimide reagent resulted in a large increase in irregular backbone structure. The backbones of PLO molecules were irregular before and after crosslinking. EDX analysis

has confirmed that PLEY fibers contained Na^+ and PLO fibers contained Br^- . The adsorption of model proteins onto PLEY fibers or PLO fibers on glass was consistent with the net charge on the proteins and the relative surface charge density of the fibers and the substrate at neutral pH. The electric field of a thick fiber is larger than that of a thin fiber for a given surface density of charge and a given distance from the fiber axis. Calculations showed that the maximum surface charge density on a peptide-based material will be less than the charge density on the outer leaflet of the plasma membrane of typical eukaryotic cells. The results, taken together, provide a foundation for analyzing the behavior of adhesive cells on electrospun fiber mats on a wettable substrate in the presence of serum. Such behavior is relevant to fiber mat applications in biotechnology and medicine, for instance, *in vitro* tissue engineering, *ex vivo* stem cell therapy, wound healing and biomaterial implantation.

Acknowledgments

We thank Ivar Giaever, Myung Kim and David Rabson for helpful discussions and the USF Mass Spectrometry/Peptide Facility and Analysis Center and the Laboratory for Advanced Materials Science and Technology for technical assistance. M.C.C. is the recipient of a fellowship from the Louis Stokes Alliance for Minority Participation-Bridge to the Doctorate program, which is supported by the National Science Foundation. This work was supported in part by Bankhead-Coley Research Foundation grant 1BC01-43279 to D.T.H.

References

1. Rutledge, G.C.; Fridrikh, S.V. Formation of fibers by electrospinning. *Adv. Drug Deliv. Rev.* **2007**, *59*, 1384–1391.
2. Sill, T.J.; von Recum, H.A. Electrospinning: Applications in drug delivery and tissue engineering. *Biomaterials* **2008**, *29*, 1989–2006.
3. Yoo, H.S.; Kim, T.G.; Park, T.G. Surface-functionalized electrospun nanofibers for tissue engineering and drug delivery. *Adv. Drug Deliv. Rev.* **2009**, *61*, 1033–1042.
4. Khadka, D.B.; Haynie, D.T. Insoluble synthetic polypeptide mats from aqueous solution by electrospinning. *ACS Appl. Mater. Interfaces* **2010**, *2*, 2728–2732.
5. Agarwal, S.; Greiner, A. On the way to clean and safe electrospinning-green electrospinning: Emulsion and suspension electrospinning. *Polym. Adv. Technol.* **2011**, *22*, 372–378.
6. Khadka, D.B.; Cross, M.C.; Haynie, D.T. A synthetic polypeptide electrospun biomaterial. *ACS Appl. Mater. Interfaces* **2011**, *3*, 2994–3001.
7. Khadka, D.B.; Haynie, D.T. Protein- and peptide-based electrospun nanofibers in medical biomaterials. *Nanomedicine* **2012**, in press.
8. Ner, Y.; Stuart, J.A.; Whited, G.; Sotzing, G.A. Electrospinning nanoribbons of a bioengineered silk-elastin-like protein (SELP) from water. *Polymer* **2009**, *50*, 5828–5836.
9. Deitzel, J.M.; Kleinmeyer, J.; Harris, D.; Beck Tan, N.C. The effect of processing variables on the morphology of electrospun nanofibers and textiles. *Polymer* **2001**, *42*, 261–272.
10. Yarin, A.L.; Koombhongse, S.; Reneker, D.H. Bending instability in electrospinning of nanofibers. *J. Appl. Phys.* **2001**, *89*, 3018–3026.

11. Minato, K.I.; Ohkawa, K.; Yamamoto, H. Chain conformations of poly(γ -benzyl-*L*-glutamate) pre and post an electrospinning process. *Macromol. Biosci.* **2006**, *6*, 487–495.
12. Hohman, M.M.; Shin, M.; Rutledge, G.; Brenner, M.P. Electrospinning and electricity forced jets. I. Stability theory. *Phys. Fluids* **2001**, *13*, 2201–2220.
13. Fridrikh, S.V.; Yu, J.H.; Brenner, M.P.; Rutledge, G.C. Controlling the fiber diameter during electrospinning. *Phys. Rev. Lett.* **2003**, *90*, 114502:1–114502:4.
14. He, J.H.; Xu, L.; Wu, Y.; Liu, Y. Mathematical models for continuous electrospun nanofibers and electrospun nanoporous microspheres. *Polym. Int.* **2007**, *56*, 1323–1329.
15. Strobl, G. *The Physics of Polymers*; Springer: Berlin, Germany, 2007.
16. Zheng, X.; Baker, H.; Hancock, W.S.; Fawaz, F.; McCaman, M.; Pungor, E. Proteomic analysis for the assessment of different lots of fetal bovine serum as a raw material for cell culture. Part IV. Application of proteomics to the manufacture of biological drugs. *Biotechnol. Prog.* **2006**, *22*, 1294–1300.
17. Chaudhuri, S.R.; Yang, J.T. Helix-coil transition of poly-*L*-ornithine in solution. *Biochemistry* **1968**, *7*, 1379–1383.
18. Wada, A. Helix-coil transformation and titration curve of poly-*L*-glutamic acid. *Mol. Phys.* **1960**, *3*, 409–416.
19. Greenfield, N.; Fasman, G.D. Computed circular dichroism spectra for the evaluation of protein conformation. *Biochemistry* **1969**, *8*, 4108–4116.
20. Wetlaufer, D. Ultraviolet spectra of proteins and amino acids. *Adv. Protein. Chem.* **1962**, *17*, 303–390.
21. Chakrabarty, A.; Kortemme, T.; Padmahabhan, S.; Baldwin, R.L. Aromatic side-chain contribution to far-ultraviolet circular dichroism of helical peptides and its effect on measurement of helix propensities. *Biochemistry* **1993**, *32*, 5560–5565.
22. Chirgadze, Y.N.; Nevskaya, N.A. Infrared spectra and resonance interaction of amide-I vibration of the antiparallel-chain pleated sheet. *Biopolymers* **1976**, *15*, 637–648.
23. Jackson, M.; Mantsch, H.H. The use and misuse of FTIR spectroscopy in the determination of protein structure. *Crit. Rev. Biochem. Mol. Biol.* **1995**, *30*, 95–120.
24. Imoto, T.; Johnson, L.N.; North, A.T.C.; Phillips, D.C.; Rupley, J.A. Vertebrate lysozymes. In *The Enzymes*; Boyer, P.D., Lardy, H., Myrback, K., Eds.; Academic: New York, NY, USA, 1972; pp. 665–868.
25. Malamud, D.; Drysdale, J.W. Isoelectric points of proteins: A table. *Anal. Biochem.* **1978**, *86*, 620–647.
26. Shenoy, S.L.; Bates, W.D.; Frisch, H.L.; Wnek, G.E. Role of chain entanglements on fiber formation during electrospinning of polymer solutions: Good solvent, non-specific polymer-polymer interaction limit. *Polymer* **2005**, *46*, 3372–3384.
27. Doty, P.; Wada, A.; Yang, J.T.; Blout, E.R. Polypeptides. VII. Molecular configurations of poly-*L*-glutamic acid in water-dioxane solution. *J. Polym. Sci.* **1957**, *23*, 851–857.
28. Zandomenighi, G.; Krebs, M.R.H.; McCammon, M.G.; Fändrich, M. FTIR reveals structural differences between native β -sheet proteins and amyloid fibrils. *Protein Sci.* **2004**, *13*, 3314–3321.

29. Richardson, J.S. The anatomy and taxonomy of protein structure. *Adv. Protein Chem.* **1981**, *34*, 167–339.
30. Laurine, E.; Gregoire, E.; Fändrich, M.; Engemann, S.; Marchal, S.; Thion, L.; Mohr, M.; Monsarrat, B.; Michel, B.; Dobson, C.M.; *et al.* Lithostathine quadruple-helical filaments from proteinase K-resistant deposits in Creutzfeldt-Jakob disease. *J. Biol. Chem.* **2003**, *278*, 51770–51778.
31. Nyquist, R.A.; Clark, T.D.; Streck, R. Infrared study of alkyl carboxylic acids in CCl₄ and/or CHCl₃ solutions. *Vib. Spectrosc.* **1994**, *7*, 275–286.
32. Baldwin, R.L. In search of the energetic role of peptide hydrogen bonds. *J. Biol. Chem.* **2003**, *278*, 17581–17588.
33. Poland, D.; Scheraga, H.A. *Theory of Helix-Coil Transition Theory in Biopolymers*; Academic: New York, NY, USA, 1970.
34. Wozniak, M.A.; Modzelewska, K.; Kwong, L.; Keely, P.J. Focal adhesion regulation of cell behavior. *Biochim. Biophys. Acta* **2004**, *1692*, 103–119.
35. Junge, K.; Binnebösel, M.; von Trotha, K.T.; Rosch, R.; Kling, U.; Neumann, U.P.; Jansen, P.L. Mesh biocompatibility: Effects of cellular inflammation and tissue remodelling. *Langenbecks Arch. Surg.* **2012**, *397*, 255–270.
36. Squires, T.M.; Brenner, M.P. Like-charge attraction and hydrodynamic interaction. *Phys. Rev. Lett.* **2000**, *85*, 4976–4979.
37. Behrens, S.H.; Grier, D.G. The charge of glass and silica surfaces. *J. Chem. Phys.* **2001**, *115*, 6716–6721.
38. Fischer, H.; Polikarpov, I.; Craievich, A.F. Average protein density is a molecular-weight-dependent function. *Protein Sci.* **2004**, *13*, 2825–2828.
39. Curtis, A.S.G.; Forrester, J.V.; McInnes, C.; Lawrie, F. Adhesion of cells to polystyrene surfaces. *J. Cell Biol.* **1983**, *97*, 1500–1506.
40. Curtis, A.S.G. Cell adhesion. *Prog. Biophys. Mol. Biol.* **1973**, *27*, 317–375.
41. Gingell, D.; Todd, I. Red blood cell adhesion. II. Interferometric examination of the interaction with hydrocarbon oil and glass. *J. Cell Sci.* **1980**, *41*, 135–149.
42. Pernodet, N.; Rafailovich, M.; Sokolov, J.; Xu, D.; Yang, N.-L.; McLeod, K.J. Fibronectin fibrillogenesis on sulfonated polystyrene surfaces. *J. Biomed. Mater. Res. A* **2003**, *64*, 684–692.
43. Harris, A.K.; Pryer, N.K.; Paydarfar, D. Effects of electric fields on fibroblast contractility and cytoskeleton. *J. Exp. Zool.* **1990**, *253*, 163–176.
44. Poo, M. *In situ* electrophoresis of membrane components. *Annu. Rev. Biophys. Bioeng.* **1981**, *10*, 245–276.
45. Sun, S.; Wise, J.; Cho, M. Human fibroblast migration in three-dimensional collagen gel in response to noninvasive electrical stimulus. I. Characterization of induced three-dimensional cell movement. *Tissue. Eng.* **2004**, *10*, 1548–1557.
46. Nuccitelli, R. A role for endogenous electric fields in wound healing. *Curr. Top. Dev. Biol.* **2003**, *58*, 1–26.
47. Borgens, R.B.; Venable, J.W., Jr.; Jaffe, L.F. Bioelectricity and regeneration: Large currents leave the stumps of regenerating newt limbs. *Proc. Nat. Acad. Sci. USA* **1977**, *74*, 4528–4532.

48. Mir, L.M.; Bureau, M.F.; Gehl, J.; Rangara, R.; Rouy, D.; Caillaud, J.M.; Delaere, P.; Branellec, D.; Schwartz, B.; Scherman, D. High-efficiency gene transfer into skeletal muscle mediated by electric pulses. *Proc. Nat. Acad. Sci. USA* **1999**, *96*, 4262–4267.
49. Hochmuth, R.M. Micropipette aspiration of living cells. *J. Biomech.* **2000**, *33*, 15–22.
50. Kinraide, T.B.; Wang, P. The surface charge density of plant cell membranes (σ): An attempt to resolve conflicting values for intrinsic σ . *J. Exp. Bot.* **2010**, *61*, 2507–2518.

© 2012 by the authors; licensee MDPI, Basel, Switzerland. This article is an open access article distributed under the terms and conditions of the Creative Commons Attribution license (<http://creativecommons.org/licenses/by/3.0/>).